

SIMULATION OF FORMING PROCESSES WITH LOCAL HEATING OF DUAL PHASE STEELS WITH USE OF LASER BEAM SHAPING SYSTEMS

R. Bielak¹, F. Bammer¹, A. Otto¹, C. Stiglbrunner¹, C. Colasse², S.P. Murzin³

¹Vienna University of Technology, Vienna, Austria,

²Faurecia Sièges d'Automobile, Caligny, France,

³Samara National Research University, Samara, Russia

Abstract

Features of laser-assisted warm forming of dual phase steel DP1000 are determined. Simulation of forming processes with local heating is performed. In the simulation procedure, the forming parameters of three dimensional forming were adapted to keep them within tolerable limits even in critical areas as well as identifying the localization and type of critical stresses. The capabilities of Abaqus were extended by use of the Python language to independently evaluate selected element strains, the position of deformed elements within the forming limit diagram and user-defined failure criteria. The simulation led to an adapted forming process permitting a significantly increased bulge forming depth by local laser heating of the forming zones. The developed simulation model shows a satisfactory conformity with experiments, performed using a fibre-coupled laser with a wavelength of 1070 nm and a maximum output power of 1500 W, and a servo bending press TRUMPF TruBend 7018. The required distribution of the laser beam energy can be obtained by using diffractive optical elements. The use of the model for technological operations opens up possibilities not only for the solution of the presented specific objective of laser assisted warm forming, but also for others applications.

Keywords: local laser heating, steel, warm forming, simulation, beam shaping system, power density distribution.

Citation: Bielak R, Bammer F, Otto A, Stiglbrunner C, Colasse C, Murzin SP. Simulation of forming processes with local heating of dual phase steels with use of laser beam shaping systems. *Computer Optics* 2016; 40(5): 659-667. DOI: 10.18287/2412-6179-2016-40-5-659-667.

Acknowledgments: The authors are grateful for useful advice and provided material data regarding the dual phase steels to Mr. Thomas Müller, Senior Manager, Forming & Machining Technology, SSAB Company, Borlänge, Sweden.

Introduction

Dual phase steels are used in the transport and automotive industries. These are characterized by a high tensile strength due to relatively hard martensitic phase and a low initial yield point due to the relatively soft ferritic phase [1–3]. Most of the research conducted in the area of the action of concentrated energy fluxes on these materials is devoted to laser welding and the study of the influence of this on the phase composition, and also properties of the welded joint [4–6]. Refs. [7, 8] show the possibility of applying laser heat treatment to increase the hardness and strength of the local areas of dual phase steels.

One of the advanced methods of processing high-strength steels are warm and hot stamping [9]. If hot forming is the forming of metal workpieces above their recrystallization temperature, then warm forming is conducted at a temperature below or near the recrystallization temperature [10, 11]. Warm forming of dual phase steels is preferred to achieve a good balance between the required forces, ductility, formability and the final product properties. The most effective is a local heating method, in which only the presumed plastic deformation zone is heated in the sheet metal forming process [12–14]. A solution can be achieved by local heating with a laser beam [15–18]. However, as a rule, researchers are studying the process of bending sheet materials with local heating, while the other schemes of stamping are rarely reported.

Use of the stamped, bearing loading details is typical for automotive industry. The profiles have to withstand big axial

and bending loads, at the same time light weight structures are required. Additional bulge forming of profiles for the purpose of formation of local deepening or cambers leads to formation of defects, cracks and considerable thinning of a wall are basic of which in some cases. In this case application of local heating is also advisable, however common recommendations for realization of this technological process are not generally available. Efficient and high-precision computer simulations based on created or improved software allows to significantly reducing the number of experimental research when developing technological processes.

The evaluation of the forming process by numerical simulation is conducted taking into account the forming limit curves (FLC) on a forming limit diagram (FLD) as well as true strain (which is defined as the natural logarithm of the ratio of the object's deformed length to its initial length) at fracture, which in fact increases with increasing temperature. It is evident from the main strain values on the ordinate axis of the FLD. Here obviously the forming limit increases with temperature. For a specific forming problem with a given material, response to temperature, an optimized temperature distribution, minimizing maximum temperature and amount of heat, can be determined. One possible way is to use the numerical simulation therefore the temperature dependence of the mechanical properties and the fracture behaviour of dual phase steels are of increasing interest [19, 20].

The used process consists of two steps, the first of which is local heating, and the subsequent second is the

mechanical forming. Ref. [21] described equipment for warm and hot laser assisted forming and shows that one approach to fit the needs of a flexible irradiation of different geometries is the usage of a galvanometer scanner. It uses two rotating mirrors to deflect the beam into the working area. However, beam scanning systems that produce a heating pattern on the treated surface by means of one- or two-axis movement of their components have significant weaknesses. These systems give a non-uniform spatial laser power distribution on the surface of the heat affected zone due to the variable speed of the beam movement and have low reliability due to the presence of mechanical parts, which are moving with high speeds [22, 23]. In contrast to such systems, diffractive optical elements (DOE) provide an opportunity to produce a laser spot as a pattern or an area with a specific distribution of laser power density [24–27].

The purpose of this research is to study of the features of laser assisted forming and development of programming scripts for the simulation of forming processes with local heating. Simulation model takes into account the specifics of the laser action on metallic materials and determine advisability of laser beam shaping by DOE for implementation of local heating before forming of dual phase steels.

Nomenclature

μ_{vs} – variable friction coefficient, μ_s ;
 μ_s – static friction coefficient - assumed to be approx. 0.125;
 $l_{cfs}(T)$ – function of temperature T ;
 $h(P)$ – transferred heat by conduction;
 k_{air} – thermal conductivity of the air in the gap as a function of temperature and is calculated by the empirical expression $k_{air} = 1.5207 \cdot 10^{-11} \cdot T^3 - 4.8574 \cdot 10^{-8} \cdot T^2 + 1.0184 \cdot 10^{-4} \cdot T - 3.9333 \cdot 10^{-4} \text{ W}/(\text{m} \cdot \text{K})$;
 λ – surface roughness - assumed to be $6.18 \cdot 10^{-5} \text{ m}$;
 σ_r – rupture stress of the blank;
 P – normal pressure;
 ϵ_{major} – current value of major principal strain;
 ϵ_{major}^{FLD} – major principal strain at damage initiation;
 ϵ_{minor} – current value of minor principal strain;
 θ, T – temperature;

R_eH – upper yield strength;
 R_eL – lower yield strength;
 R_m – tensile strength;
 $R_{p0.2}$ – yield strength (0.2% yield point);
 A_{80} – elongation after fracture;
 K – strength coefficient;
 n – strain hardening exponent.

1. The material under study

A commercial DP1000 steel has been used in this study. The chemical composition of the material is given below in Table 1. The thickness of the metallic material was $d=1.5 \text{ mm}$. The thermal properties of DP1000 steel, as used for the thermal simulation described later, are documented in Table 2. The properties at elevated temperatures were defined for the temperature range of $400 - 830^\circ\text{C}$ to cover the applicable temperatures of forming. The influence of local heating below 500°C on the forming process is negligible; increase of temperatures from around 800°C up, depending on the specific type of steel, cause changes of the microstructure [15], which it is undesirable. Numerical simulation of the laser heating and forming of the metallic material requires knowledge of the mechanical properties at elevated temperatures, shown in Table 3. The information about the mechanical properties has been provided by SSAB [28]. All measurement procedures follow currently valid ISO standards [29].

Table 1. Chemical composition of the DP1000 steel, max wt%

Chemical element	C	Si	Mn	P	S
max wt%	0.18	0.8	1.8	0.02	0.01
Chemical element	Al	Nb-Ti	Cr-Mo	B	Cu
max wt%	0.015–1.0	0.1	1.4	0.005	0.2

Table 2. Density ρ , specific heat capacity c_p , thermal conductivity λ_k , thermal diffusivity $a = k/(\rho c_p)$ of the DP1000 steel at room and elevated temperatures

$T [^\circ\text{C}]$	$\rho [\text{kg}/\text{m}^3]$	$c_p [\text{J}/(\text{kg} \cdot \text{K})]$	$k [\text{W}/\text{m} \cdot \text{K}]$	$a [\text{mm}^2/\text{s}]$
20	7873	470	66.9	18.1
200	7817	565	56.4	12.8
400	7749	650	46.1	9.2
600	7676	825	37.3	5.9

Table 3. Mechanical properties of steel DP1000 at room and elevated temperatures

$T [^\circ\text{C}]$	$R_eH [\text{MPa}]$	$R_eL [\text{MPa}]$	$R_{p0.2} [\text{MPa}]$	$R_m [\text{MPa}]$	$A_{80} [\%]$	n	K
20			638	1011	14	0.143	1554
400	754	744	746	903	12	0.090	1238
500	780	758	760	852	15	0.086	1147
600	740	688	688	753	14	0.098	1046
720	658	609	612	671	17	0.115	960
780	578	552	555	619	21	0.149	958
830	504	494	496	651	22	0.188	1088

2. Finite elements simulation

Finite elements analysis software Abaqus 6.14 [30] was used to calculate of the temperatures and mechanical loading. Fully coupled temperature-displacement analysis was considered i.e. at every time increment, temperature and displacement were calculated at each node simultaneously. All steps in Abaqus were conducted with the standard implicit solver.

2.1. Heating simulation

For uncoupled and coupled simulations during separate and simultaneous calculations, thermal properties of the material (Table 2) as well as the mechanical ones (Table 3) were considered in the model. The temperature field, caused by the laser irradiation, was calculated incorporating heat conduction, while the heat input was modelled as a surface heat flow.

It was determined that absorption increases significantly during laser action due to a fast growing oxide layer. In the case under consideration modeling was performed assuming a linear increase of the absorption coefficient from 30 % to 75 % in the temperature range from 350 °C to 500 °C. Calculation of the free model parts cooling (i.e. parts without contact to each other) was performed taking into account a combined heat transfer coefficient (Table 4), which is the sum of the convection and radiation heat transfer coefficients.

Table 4. Combined convection and radiation heat transfer coefficient H_{comb} / cooling to air

$T [^{\circ}\text{C}]$	0	400	800	1200
$H_{comb} [\text{W m}^{-2}\text{K}^{-1}]$	13.4	30.7	78.3	172

2.2. Forming simulation

The tool-material with relatively low and constant heat conductivity 11.6 W/m K, density 7850 kg/m³, and thermal capacity 450 J/kg K was chosen. The tool has been modeled of the so-called rigid body elements that simulate behavior of hard, non-deformable material. For the profile 11100 shell elements (S4RT) have been defined with a thickness of 1.5 mm splitted into 5 virtual layers. A fully coupled temperature-displacement procedure was used to determine stress, strain, displacement, and temperature fields simultaneously.

Strength and hardness of the contact surfaces, properties of the oxide film covering the blank surface and the lubrication oil (if any) are the key factors that determine the friction coefficient. The Shvets-Dyban [31] friction expression was being utilized to simulate the friction coefficient in the contact area between the blank and tools. The thermal contact conductance is the most critical parameter controlling cooling of the profile during forming and has the greatest uncertainty. Values are stated in [32] for several metals with various surface roughnesses as a function of interface pressure. Coefficients taking into account the influence of lubricants are also included. Transferred heat by conduction, used in our simulation case are based on Shvets formula [31]:

$$h(P) = (k_{air} \pi / 4 \lambda_{ra}) \cdot [1 + 85 (P / \sigma_r)^{0.8}], \quad (1)$$

λ_{ra} – surface roughness – assumed to be $6.18 \cdot 10^{-5}$ m.

2.3. Damage evaluation

The FLC is the connecting line of states above which deformation becomes unstable. It shows the limits of the formability of a sheet of material. The FLD damage initiation criteria were specified in Abaqus input file of the FLC in tabular form by stating the major principal strain at damage initiation as a tabular function of the minor principal strain and temperature additionally. Strains computed numerically were compared to a FLC to determine the feasibility of the forming process under analysis.

The FLD damage initiation criterion is defined by the condition $\omega_{FLC} = 1$, where the variable ω_{FLC} (damage initiation criterion) is a function of the current deformation state. ω_{FLC} was defined as:

$$\omega_{FLC} = \varepsilon_{major} / [\varepsilon_{major}^{FLC} (\varepsilon_{minor}, \theta)]. \quad (2)$$

Damage calculation, based on FLD criteria, is not supported by all element types, therefore an alternative data acquisition has been developed.

This approach uses the Abaqus Python script environment to access result (*.odb) files and extract results on element and node level for each simulation time step. The actual nodal coordinates of selected elements are compared to the initial ones and differences (corresponds to element deformation) are used to calculate the minor and major strains in accordance to [29]. Finally, each calculated minor and major strain result of deformed elements is being rendered within the appropriate FLC diagram, considering time steps as well the respective actual element temperature.

3. Simulation results and analysis

Main objective of the simulation was to determine the laser beam intensity distribution as well as time and position of heat input to find the maximal forming depth avoiding rupture of the material. The simulation was performed for two kinds of forming processes, with laser heating (warm forming) and without heating (cold forming). In the case of warm forming the profile was firstly heated up to 800 °C (approximately 12 seconds) and formed subsequently. Unheated material was formed at room temperature. Fig. 1 shows the final deformed shape of the profile and the thermal field, calculated at the final stage of laser assisted warm forming process.

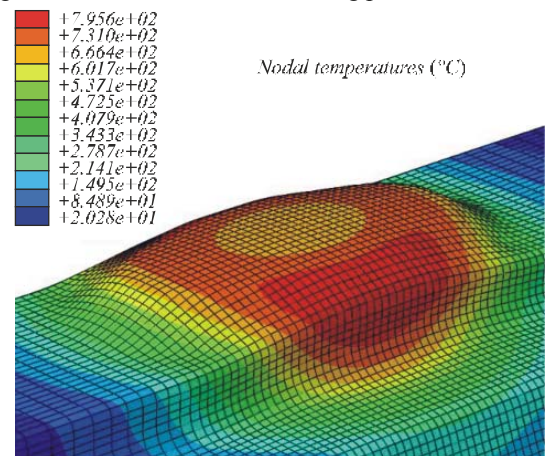


Fig. 1. Temperature field, caused by elliptical ring shaped laser beam irradiation at the first stage of the forming process; the profile has been irradiated 12 seconds with the constant intensity of 2.24 W/mm²; temperature field is displayed on finally deformed shape

Time-history temperature profile of node with the maximal temperature, brings the Fig. 2. The curve progression is very similar for all irradiated nodes and reflects the increasing of absorption coefficient from 30 % to 75 %, based on actual local temperature, recalculated at every iteration for every single node.

In both forming cases, the punch was moved into the formed profile following a 4 mm trajectory. For both the damage initiation criterion for the FLC exceeded the value 1 or 100 % (rupture limit was reached). Differences emerged for the respective depth of forming showing an initiation of cracks.

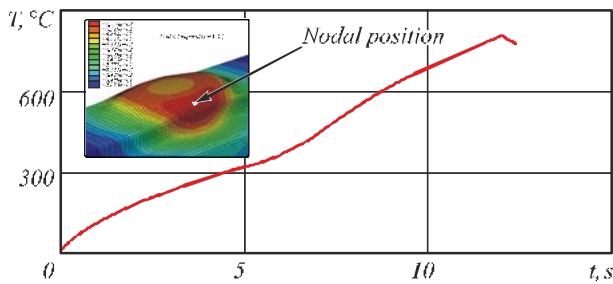


Fig. 2. Example of the time-history temperature curve of node with maximal temperature

The red elements show positions of possible rupture during cold bulge forming (Fig. 3a) and warm bulge forming (Fig. 3b). Fig. 4 shows the depth of forming operation with the first failure occurrence. In the case of cold forming displacement corresponds to a depth of 2.202 mm (a) and 3.583 mm for laser assisted forming (b).

The new model offers ways of very detailed study of the forming process. In Fig. 5 the state of the highlighted element during the forming process is indicated by circular points (red colour for the heated and blue for the cold deformation). During the forming process they obviously

move up from low to increased major strain, this at the same time being the chronologically ordered. An investigation of different single elements and the strains they are subjected to during deformation shows very diverse results comparing the cold forming process to the laser heated. Fig. 5, a highlights an element that is hardly being subjected to major strain for cold, while the contrary is the case for the heated deformation. Fig. 5b shows an element for which the opposite is true. The selected element in Fig. 5c is hardly subjected to major strain for either type of deformation, while the one of Fig. 5d is both cases clearly demonstrates the exceeding of rupture limit in both simulated cases.

Fig. 5 does not offer an overall conclusion about formability, it rather demonstrates that the critical elements for the different types of deformation can be found at different spatial positions. For the case described here an irradiation with 1500 W power for a duration of 12 s turned out to be optimal as the quite long irradiation time results in a quite homogeneous temperature field over the cross-section of the sheet without exceeding temperatures of $\sim 800\text{--}900^\circ\text{C}$ which are allowed in maximum without significantly deteriorating the material properties.

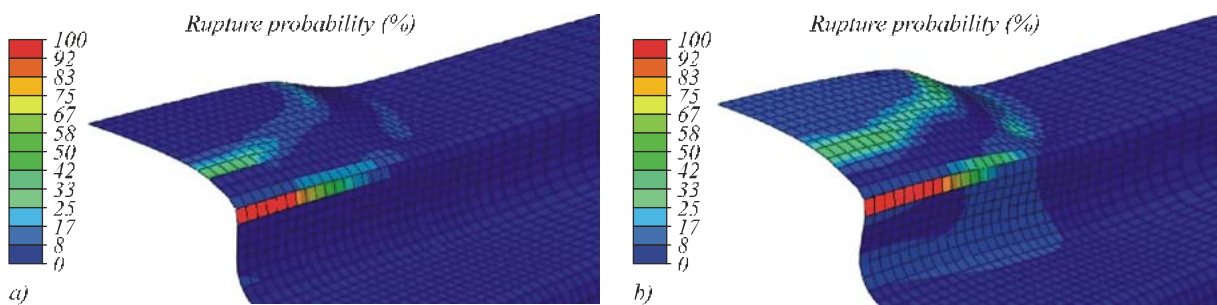


Fig. 3. Position of elements with positive rupture criteria in the case of cold (a) and laser assisted forming (b)

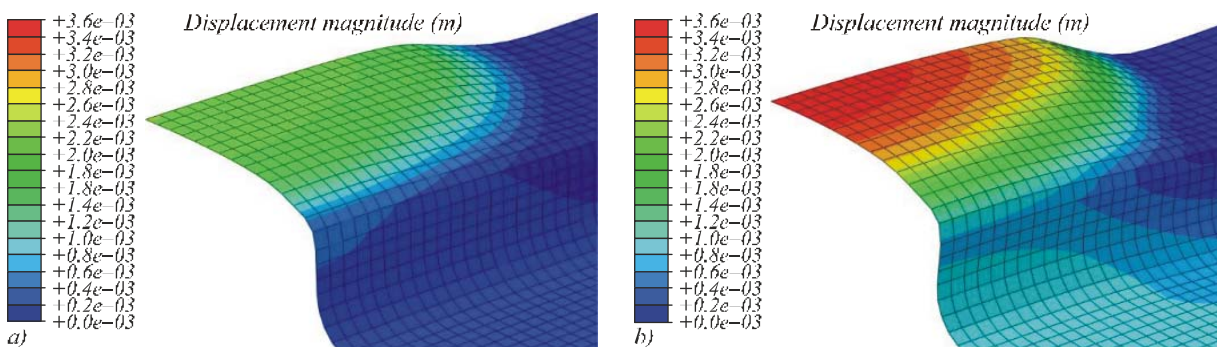


Fig. 4. Displacement magnitude of the formed steel profile at rupture probability threshold in cold (a) and laser assisted forming (b); it was reached at the forming depth of 2.2 mm in the case of cold forming (a) and at significantly superior 3.6 mm in the case of laser assisted warm forming (b)

4. Experimental study

4.1. Laser, optics and forming tool

The laser source was a fibre-coupled laser with a wavelength of 1070 nm and a maximum output power of 1500 W. In order to resemble the target zone the beam was transformed to an elliptical ring by optics consisting of a plano-convex lens with focus of 100 mm and an axicon, which was projected onto the surface at an angle of 45° . The plano-convex lens is part of the optical scheme of laser machining system that serially manufactured.

Output beam diameter $d_b = 12$ mm. Axicon from material BK7 was a lens with the one a flat side and other a conical side [33], lens diameter 40 mm, edge thickness 8.0 mm, coated AR/AR at 1070 nm, $\text{AOI} = 0^\circ$. Fig. 6 shows experimental optical scheme that was settings: apex angle $\beta = 163^\circ$, axicon angle $\alpha = 8.50^\circ$. Distance from the axicon to the center of the working plane $L = 180$ mm. The thickness of the ring in a plane perpendicular to the direction of propagation beam $h = 6$ mm, angle of divergence of ring beam $\varphi = 7.65^\circ$. External and

internal diameter of a ring, respectively, $B_1=26.7$ mm and $B_2=10.7$ mm.

Outer borders of this ring were defined by parameters $A_1=38$ mm and $B_1=26.7$ mm, and inner borders were defined by $A_2=15.2$ mm and $B_2=10.7$ mm, shifted by $D=0.76$ mm against the outer ellipse. Due to the relatively high beam divergence angle of the axicon, at the edges of processing area takes place a reduction of power density of not less than 10%. However, this reduction in power density has almost no effect on the results of laser assisted warm forming. Hence the power density distribution is modelled as of constant intensity

$I_{las}=2.24$ W/mm² at 1500 W total for the ring zone of 670 mm² and zero beyond. As discussed later absorption is increasing from 30% to 75%, resulting in $I_{abs}=0.67-1.68$ W/mm² absorbed. This corresponds to temperature-change-rates of $I_{abs}/c_p/\rho/d=\sim 100-300$ K/s, provided in-depth heat-conduction is infinite and the lateral is zero, as all other losses (ρ, c_p). The experiments were realized on a servo bending press (TRUMPF TruBend 7018, max. force 180 kN). The forming tool was provided by Faurecia Sieges d'Automobile. Fig. 7 shows the whole setup, the press, the bulge forming tool, the laser head and the optics.

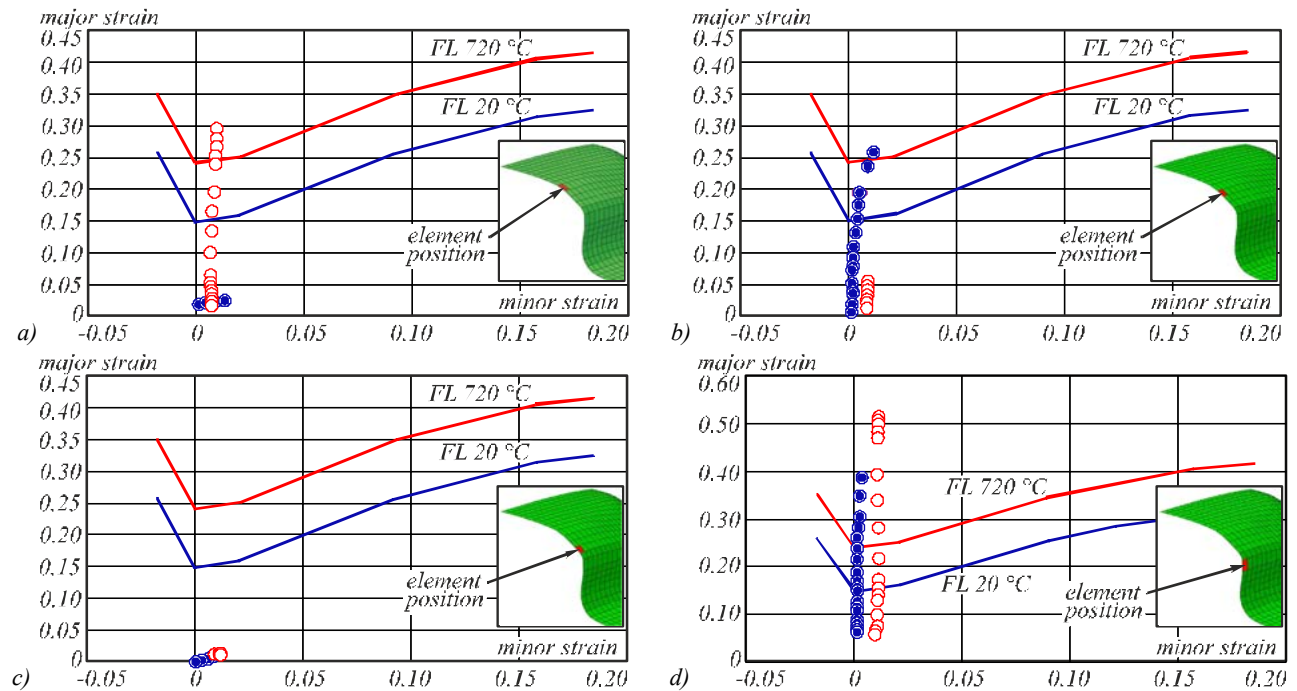


Fig. 5. Position of 4 (a, b, c and d) selected elements during cold (blue points) and laser assisted (red points) forming within stress-strain diagram with forming limit curves; - characterizing the degree of deformation with respect to FLC; geometrical position (green mesh) of the element highlighted in red; continuous lines indicate the forming limits of warm (red colour) and cold (blue colour) forming limits and circular spots (again red for warm and blue for cold) indicate the chronological sequence of the deformation state of the element

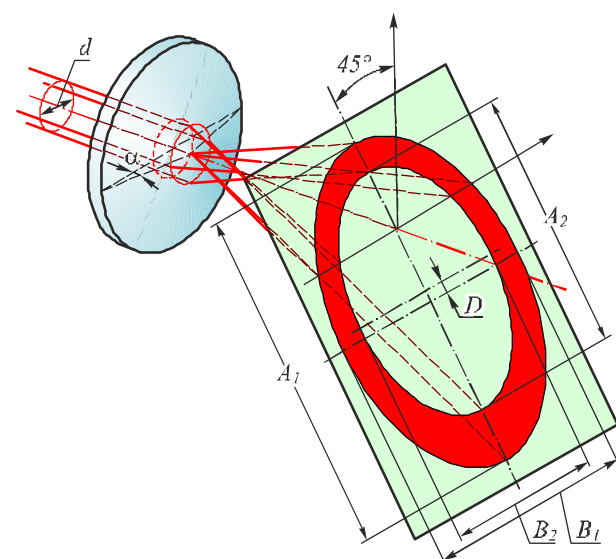


Fig. 6. Experimental optical scheme

Outer borders of this ring were defined by parameters $A_1=38$ mm and $B_1=26.7$ mm, and inner borders were defined by $A_2=15.2$ mm and $B_2=10.7$ mm, shifted by $D=0.76$ mm against the outer ellipse. Due to the relatively high beam divergence angle of the axicon, at the edges of processing area takes place a reduction of power density of not less than 10%. However, this reduction in power density has almost no effect on the results of laser assisted warm forming. Hence the power density distribution is modelled as of constant intensity $I_{las}=2.24$ W/mm² at 1500 W total for the ring zone of 670 mm² and zero beyond. As discussed later absorption is increasing from 30% to 75%, resulting in $I_{abs}=0.67-1.68$ W/mm² absorbed. This corresponds to temperature-change-rates of $I_{abs}/c_p/\rho/d=\sim 100-300$ K/s, provided in-depth heat-conduction is infinite and the lateral is zero, as all other losses (ρ, c_p). The experiments were realized on a servo bending press (TRUMPF TruBend 7018, max. force 180 kN). The forming tool was provided by Faurecia Sièges Automobiles. Fig. 7 shows the whole setup, the press, the bulge forming tool, the laser head and the optics.

4.2. Experiment

The experiments were performed at 1500 W of laser power, applying varied heating times. The intensity distribu-

tion was matched to the forming zone. Fig. 8 shows a sequence of the process. After heating, the upper tool is being moved down with ~ 100 kN force and 10 mm/s speed.

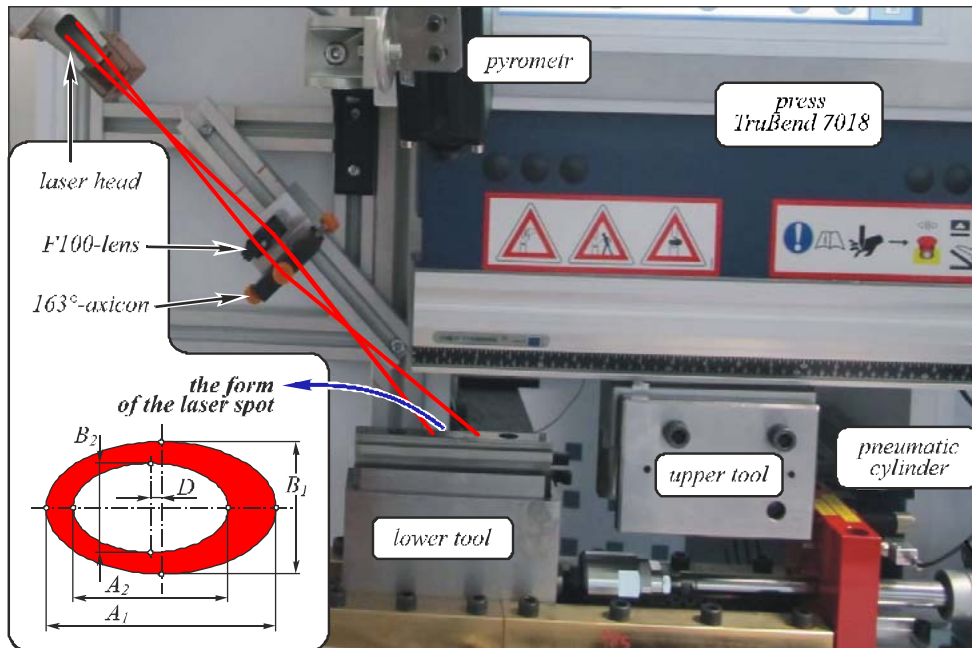


Fig. 7. The experimental setup

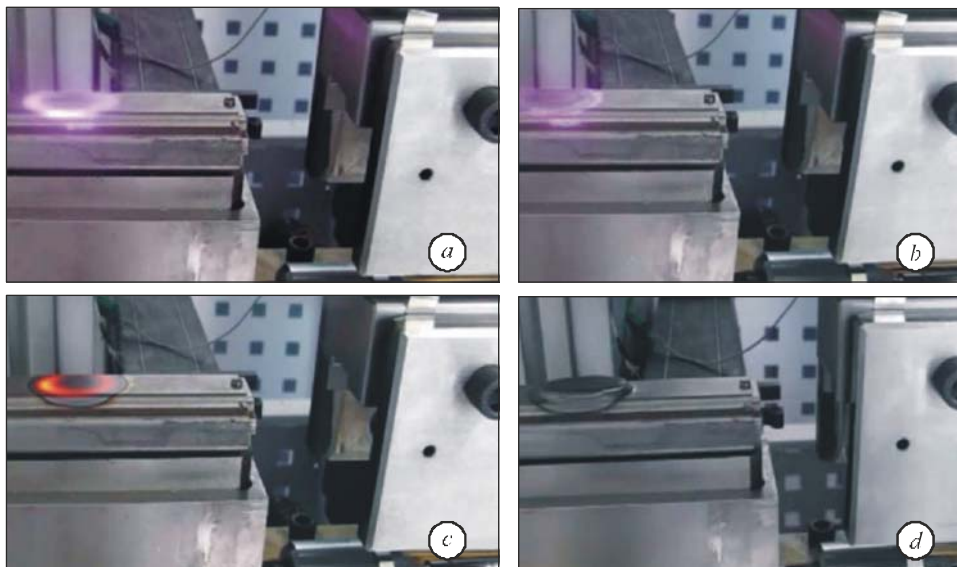


Fig. 8. Sequence of the forming process; (a) beginning of laser heating with diffusively reflected laser beam; (b) absorption has increased and the reflected laser light becomes weaker; (c) distinctive glowing after heating has terminated; (d) final result after bulge forming

Very good matching between the simulation model and the cracks caused by the real forming process can be observed in Fig. 9.

Appearance of cracks in the peripheral regions of plastic deformation zone could be explained as follows:

In these areas the work piece goes to the not uniformly tight contact with the tool. Friction contact forces, created during the sliding movement between the formed profile and the punch are lower, in comparison to the friction forces in the central region. These forces act against the deformation with the less intensity, compared to central ones.

Known method of elimination of ruptures during the forming with the cylindrical punch side by side to preliminary formed work piece in the form of circular channel between the blank and holder is the flange selective heating. In this case the Doughnut laser beam shape was used.

Heating with the homogenous circular heat source with the uniform energy intensity, so called Top Hat, could be recommended

Performed simulation of laser assisted warm forming with Top Hat laser beam profile with the radius of 22 mm projected onto the surface at an angle of 45° and the same

absorbed energy, as by Doughnut laser beam shape irradiation, $0.67 - 1.68 \text{ W/mm}^2$ absorbed. Herewith the heating time was reduced below 4 seconds and forming depth 4 mm was reached too. Conditions for disruption creation, reported as damage criteria, were not reached (forming limit damage criteria $\text{FLDCRT} < 1$).

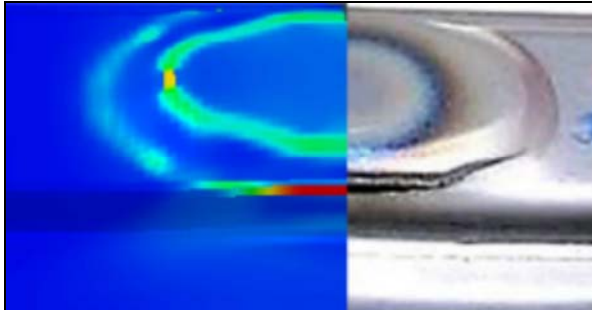


Fig. 9. Comparison of calculated rupture probability threshold (left) with the real experimental output (right); the rupture was caused by the low temperature, due to insufficient heating time 5 s; depth at rupture 3.5 mm

Experimental results confirmed this calculated prediction. However, the wall thinning near 22% may be not acceptable in work piece work conditions. Fig. 10 shows the simulation result of laser assisted warm forming with the Top Hat heat source and detailed view on workpiece.

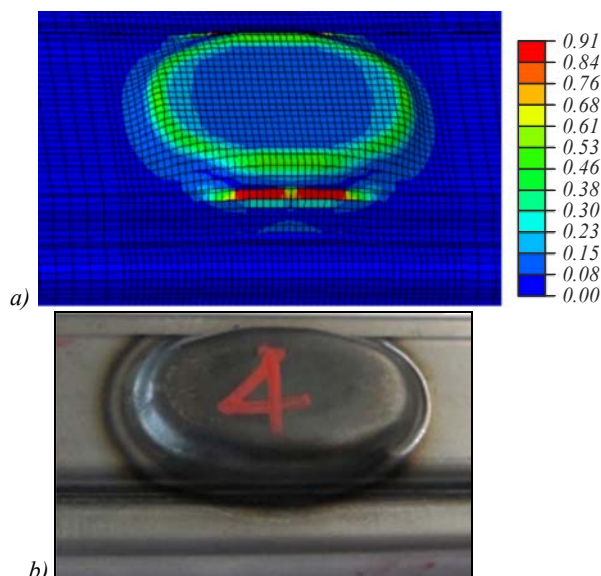


Fig. 10. The simulation result of laser assisted warm forming with the Top Hat heat source (a) and detailed view on workpiece (b)

Optimization of heat source will allow to perform laser assisted warm forming without the described defects. In a such technological processes, the special optics has to be used. It is required a more precise local dosage of energy supply of the laser beam into the heat affected zone with the possibility of power density redistribution. Such redistribution of the laser beam energy may be obtained by DOEs [34], which application in technological operations opens perspectives not only for the solution of the presented specific objective of laser assisted warm forming, but also for others applications.

Typical applications of presented solutions in laser assisted warm forming are: child seats for cars, train seats, ladders, bumpers, truck load stays, transport cages, tubes etc. Fig. 11. shows a typical seat rail.

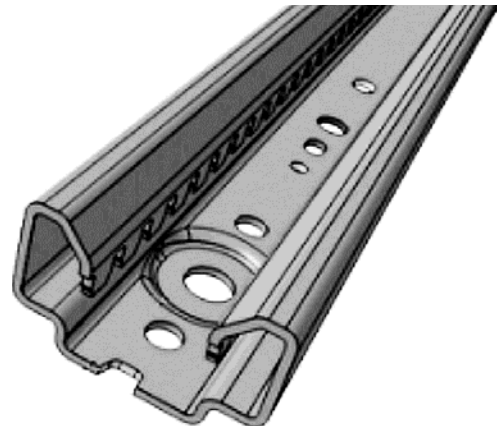


Fig. 11. Rail for the car seat

The depth of the forming area of this rail (providing space for the head of the screw fixing the rail to the floor plate) is 3.5 mm in this case, requiring a high forming rate in the peripheral parts of the formed area, so that currently only weaker steels can be used for these seat-rails. By switching to grade DP1000 the thickness could be reduced from currently 1.8 to 1.5 mm resulting in 17% reduction of weight. This material however cracks being subjected to cold-forming and therefore needs local heating. Laser-heating was chosen due to its quality to concentrate energy in small regions.

Conclusions

Local laser heat treatment has the potential to improve the form-ability of grade DP1000 steels. Both experimental and simulation results confirm possible increase of 50% in depth in comparison to cold forming.

Spatial position and temporal gradient of laser beam irradiation, especially in the case of complex geometry, shows an enormous influence on the forming process. Improvement of forming and heating parameters and thus the developing time and costs of the forming tools can be successfully reduced by numerical simulation. The developed simulation model shows satisfactory conformity with experiments.

The developed simulation model combines advanced modeling techniques (temperature dependent thermo-mechanical properties, thermal and pressure dependent contact properties, temperature dependent of laser beam absorption) with user programmed modules (evaluation of the simulation output by user defined criteria).

Dual phase steels are structurally sensitive materials. Processing of such materials requires a more precise local dosage of energy supply of the laser beam into the heat affected zone with the possibility of power density redistribution. Such redistribution of the laser beam energy may be obtained by DOEs, which application in technological operations opens perspectives not only for the solution of the presented specific objective of laser assisted warm forming, but also for others applications.

References

- [1] Al-Abbasi FM, Nemes JA. Characterizing DP-steels using micromechanical modeling of cells. *Comp Mater Sci* 2007; 39(2): 402-415. DOI: 10.1016/j.commatsci.2006.07.003.
- [2] Amirmaleki M, Samei J, Green DE, van Riemsdijk I, Stewart L. 3D micromechanical modeling of dual phase steels using the representative volume element method. *Mech Mater* 2016; 101: 27-39. DOI: 10.1016/j.mechmat.2016.07.011.
- [3] Huang TT, Gou RB, Dan WJ, Zhang WG. Strain-hardening behaviors of dual phase steels with microstructure features. *Mat Sci Eng A* 2016; 672: 88-97. DOI: 10.1016/j.msea.2016.06.066.
- [4] Farabi N, Chen DL, Zhou Y. Microstructure and mechanical properties of laser welded dissimilar DP600/DP980 dual-phase steel joints. *J Alloy Compd* 2011; 509(3): 982-989. DOI: 10.1016/j.jallcom.2010.08.158.
- [5] Farabi N, Chen DL, Zhou Y. Tensile properties and work hardening behavior of laser-welded dual-phase steel joints. *J Mater Eng Perform* 2011; 21(2): 222-230. DOI: 10.1007/s11665-011-9865-8.
- [6] Jia Q, Guo W, Li W, Zhu Y, Peng P, Zou G. Microstructure and tensile behavior of fiber laser-welded blanks of DP600 and DP980 steels. *J Mater Process Tech* 2016; 236: 73-83. DOI: 10.1016/j.jmatprotec.2016.05.011.
- [7] Kong F, Santhanakrishnan S, Kovacevic R. Numerical modeling and experimental study of thermally induced residual stress in the direct diode laser heat treatment of dual-phase 980 steel. *Int J Adv Manuf Tech* 2013; 68(9-12): 2419-2430. DOI: 10.1007/s00170-013-4859-3.
- [8] Asadi M, Frommeyer G, Aghajani A, Timokhina I, Palkowski H. Local laser heat treatment in dual-phase steels. *Metall Mater Trans A* 2012; 43(4): 1244-1258. DOI: 10.1007/s11661-011-0943-1.
- [9] Karbasian H, Tekkaya AE. A review on hot stamping. *J Mater Process Tech* 2010; 210(15): 2103-2118. DOI: 10.1016/j.jmatprotec.2010.07.019.
- [10] Mori K, Maki S, Tanaka Y. Warm and hot stamping of ultra tensile strength steel sheets using resistance heating. *CIRP Ann-Manuf Techn* 2009; 54(1): 209-212. DOI: 10.1016/S0007-8506(07)60085-7.
- [11] Tong L, Stahel S, Hora P. Modeling for the FE simulation of warm metal forming processes. *AIP Conference Proceedings: NUMISHEET 2005*; 778: 625. DOI: 10.1063/1.2011292.
- [12] Park JC, Seong DY, Yang DY, Cha MH. Development of an innovative bending process employing synchronous incremental heating and incremental forming. In: Hirt G, Tekkaya AE, eds. *Special Edition: 10th International Conference on Technology of Plasticity, ICTP 2011*. Weinheim: Wiley-VCH Verlag GmbH & Co; 2011.
- [13] Lee E-H, Hwang J-S, Lee C-W, Yang D-Y, Yang W-H. A local heating method by near-infrared rays for forming of non-quenched advanced high-strength steels. *J Mater Process Tech* 2014; 214(4): 784-793. DOI: 10.1016/j.jmatprotec.2013.11.023.
- [14] Lee E-H, Yang D-Y, Yoon JW, Yang W-H. Numerical modeling and analysis for forming process of dual-phase 980 steel exposed to infrared local heating. *Int J Solids Struct* 2015; 75-76: 211-224. DOI: 10.1016/j.ijsolstr.2015.08.014.
- [15] Neugebauer R, Scheffler S, Poprawe R, Weisheit A. Local laser heat treatment of ultra high strength steels to improve formability. *Prod Eng* 2009; 3(4-5): 347-351. DOI: 10.1007/s11740-009-0186-9.
- [16] Romero P, Otero N, Cabrera J, Masague D. Laser assisted conical spin forming of dual phase automotive steel. experimental demonstration of work hardening reduction and forming limit extension. *Physics Procedia* 2010; 5: 215-225. DOI: 10.1016/j.phpro.2010.08.047.
- [17] Bammer F, Holzinger B, Humenberger G, Schuöcker D, Schumi T. Integration of high power lasers in bending tools. *Physics Procedia* 2010; 5: 205-209. DOI: 10.1016/j.phpro.2010.08.045.
- [18] Bammer F, Schumi T, Otto A, Schuöcker D. Laser assisted bending for efficient light-weight-production. *Tehnicki Vjesnik* 2001; 18(4): 571-576.
- [19] Wu-rong W, Chang-wei H, Zhong-hua Z, Xi-cheng W. The limit drawing ratio and formability prediction of advanced high strength dual-phase steels. *Materials and Design* 2011; 32(6): 3320-3327. DOI: 10.1016/j.matdes.2011.02.021.
- [20] Hug E, Martinez M, Chottin J. Temperature and stress state influence on void evolution in a high-strength dual-phase steel. *Mat Sci Eng A* 2015; 626: 286-295. DOI: 10.1016/j.msea.2014.12.053.
- [21] Brecher C, Emonts M, Eckert M. Laser-assisted sheet metal working by the integration of scanner system technology into a progressive die. *Physics Procedia* 2012; 39: 249-256. DOI: 10.1016/j.phpro.2012.10.036.
- [22] Murzin SP. Local laser annealing for aluminium alloy parts. *Laser Eng* 2016; 33(1-3): 67-76.
- [23] Murzin SP. Formation of structures in materials by laser treatment to enhance the performance characteristics of aircraft engine parts. *Computer Optics* 2016; 40(3): 353-359. DOI: 10.18287/2412-6179-2016-40-3-353-359.
- [24] Doskolovich LL, Kazanskiy NL, Soifer VA. DOE for focusing the laser light. In book: Soifer VA, ed. *Methods for computer design of diffractive optical elements*. New York: John Wiley & Sons Inc.; 2002. ISBN: 978-0-471-09533-8.
- [25] Alferov SV, Karpeev SV, Khonina SN, Tukmakov KN, Moiseev OYu, Shulyapov SA, Ivanov KA, Savel'ev-Trofimov AB. On the possibility of controlling laser ablation by tightly focused femtosecond radiation. *Quantum Electronics* 2014; 44(11): 1061-1065. DOI: 10.1070/QE2014v044n11ABEH015471.
- [26] Soifer VA, Kotlyar VV, Khonina SN, Skidanov RV. Remarkable laser beams formed by computer-generated optical elements: properties and applications. *Proc SPIE* 2006; 6252: 62521B. DOI: 10.1117/12.677054.
- [27] Pavelyev VS, Borodin SA, Kazanskiy NL, Kostyuk GF, Volkov AV. Formation of diffractive microrelief on diamond film surface. *Opt Laser Technol* 2007; 39(6): 1234-1238. DOI: 10.1016/j.optlastec.2006.08.004.
- [28] SSAB, 2012. Mechanical properties of heat treated steel, Technical Report N1.97BC.07.0178, 2012.
- [29] ISO 12004-2:2008, 2008. Metallic materials – Sheet and strip – Determination of forming-limit curves – Part 2: Determination of forming-limit curves in the laboratory. ISO/TC 164/SC 2. ICS: 77.040.10. Stage: 90.93.
- [30] Abaqus, 2014, Version 6.14. Documentation.
- [31] Shvets IT. Contact heat transfer between plane metal surfaces. *International Chemical Engineering* 1964; 4(4): 621-624.
- [32] Yanagida A, Azushima A. Evaluation of coefficients of friction in hot stamping by hot flat drawing test. *CIRP Ann-Manuf Techn* 2009; 58(1): 247-250. DOI: 10.1016/j.cirp.2009.03.091.
- [33] Ustinov AV, Khonina SN. Calculating the complex transmission function of refractive axicons. *Optical Memory and Neural Networks (Information Optics)* 2012; 21(3): 133-144. DOI: 10.3103/S1060992X1203006X.
- [34] Doskolovich LL, Khonina SN, Kotlyar VV, Nikolsky IV, Soifer VA, Uspleniev GV. Focuser into a ring. *Optical and Quantum Electronics* 1993; 25(11): 801-814. DOI: 10.1007/BF00430188.

Authors' information

Robert Bielak (b. 1969) graduated from the Slovak Technical University in 1992, majoring in Welding Technology where received his PhD degree in 1999. He is holding the position of a project assistant at the Institute for Production En-

gineering and Laser Technology at the Vienna University of Technology. His research interests are currently focused on lasers and laser assisted processes. He is co-author of more than 70 scientific papers. E-mail: robert.bielak@tuwien.ac.at .

Ferdinand Bammer (b. 1976) graduated from the Vienna University of Technology 1998 majoring in Mechanical Engineering where he also received his Doctor in Engineering Science in 2000 and habilitation treatise in 2009. Has been working in the field of industrial laser applications at the Vienna University of Technology since 2001. He worked in various fields like laser-pulsing, laser-assisted forming, and ellipsometry. He is co-author of more than 90 scientific papers. E-mail: f.bammer@tuwien.ac.at .

Andreas Otto (b. 1966) graduated from the Friedrich-Alexander University Erlangen, Germany in 1992 majoring in Physics where he also received his Doctor in Engineering Science in 1996. After several years as Senior Scientist he was called to Vienna University of Technology as Full Professor in 2011. Since then he is Head of the Group for Laser and Laser Assisted Manufacturing at the Institute for Production Engineering and Laser Technology. He is author respectively co-author of more than 250 scientific papers and holds several patents. E-mail: andreas.otto@tuwien.ac.at .

Christian F. Stiglbrunner (b. 1955) graduated from the Vienna University of Technology 1984 majoring in Industrial Engineering. After several positions in the industry he returned to the University, currently holding the position of a project assistant at the Institute for Production Engineering and Laser Technology at Vienna University of Technology. His research interests are focused on lasers and laser machining. He is co-author of more than 10 scientific papers. E-mail: christian.stiglbrunner@tuwien.ac.at .

Claude Colasse (b.1959) graduated BTS Fab Meca, 1981 in France, started at Faurecia Group in 1982. His product / process experience led him to become the process pilot manager of the start-up of new track products for car seats. His involvement also led him to assist the Canadian plant when tracks production started over there. In 2001 he joined the Advanced Engineering department and develop new bending and laser welding Technologies for specific applications. He has become an authority on materials used in stamping processes, especially for the bending tools. Promoted stamping Expert in 2007, he has developed validation procedures for tools and materials, written specifications books for special technics. He gave lectures in four international conferences about tooling steels applications. Working for Innovation Dept., he is author of 14 patents for Faurecia group.

Serguei Petrovich Murzin (b. 1963) graduated (1986) from S.P. Korolyov Kuibyshev Aviation Institute (KuAI, presently, Samara National Research University, short – Samara University) majoring in Aircraft Engines. He received his Doctor in Technics (2005) degree from Samara National Research University. He is holding the position of a professor in Samara University at the department of Automatic Systems of Power Plants. He is the head of the Research & Education Center of Laser Systems and Technologies. He is a specialist in laser technology and nanotechnology, laser physics and optics. He is a co-author of over 90 scientific papers, two monographs, and 18 inventions and patents. E-mail: murzin@ssau.ru .

Code of State Categories Scientific and Technical Information (in Russian – GRNTI): 29.33.47.

Received September 7, 2016. The final version – October 31, 2016.
